Supporting Information

Zhang et al. 10.1073/pnas.1505531112

SI Materials and Methods

Ncd Protein Expression and Purification. The Ncd pET/MC1 plasmid (1, 2) was a generous gift of Sharyn A. Endow (Duke University Medical Center, Durham, NC) and was expressed in *E. coli* BL21-CodonPlus (DE3)-RIL cell line (Stratagene) for purification as described previously (2, 3). Cells were grown in lysogeny broth (LB) with antibiotics (75 μg/mL ampicillin, 10 μg/mL chloramphenicol) at 37 °C until A_{600} was ∼0.4, and then the cells were cooled on ice to 16 °C, followed by induction with 75 μM isopropyl β-D-1-thiogalactopyranoside. Protein expression was continued for 16 h at 16 °C with shaking, followed by centrifugation. The cell pellets were resuspended in lysis buffer (10 mM sodium phosphate buffer, pH 7.2, 30 mM NaCl, 5 mM $MgCl_2$, 1 mM EGTA, 1 mM EDTA, 10 mM phenylmethylsulfonyl fluoride, 1 mM DTT, and 0.02 mM ATP) at 10 mL/g wet weight, and adjusted to 0.1 mg/mL lysozyme. The cells were incubated for 45 min at 4 °C with gentle stirring. Following three cycles of freezing (liquid N_2) and thawing (37 °C), the lysates were clarified by ultracentrifugation. The supernatant was loaded onto a SP Sepharose column (HiTrap SP FF; GE Healthcare Life Sciences) that was preequilibrated in SP Sepharose binding buffer (10 mM sodium phosphate buffer, pH 7.2, 30 mM NaCl, 5 mM $MgCl_2$, 0.1 mM EGTA, 0.1 mM EDTA, 1 mM DTT, 0.02 mM ATP). After washing with the binding buffer, the proteins were eluted from the column with a linear gradient of 30–600 mM NaCl in Sepharose binding buffer. Fractions containing Ncd MC1 were identified by SDS/PAGE, pooled, and dialyzed against diethylaminoethyl (DEAE) column binding buffer (10 mM sodium phosphate buffer, pH 7.2, 30 mM NaCl, 2 mM $MgCl_2$, 0.1 mM EGTA, 0.1 mM EDTA, 1 mM DTT, 0.02 mM ATP). The dialyzed proteins were loaded onto a preequilibrated DEAE column (HiTrap DEAE FF; GE Healthcare) and the column was washed with DEAE column binding buffer, followed by protein elution with a linear gradient of 30–400 mM NaCl in the DEAE column binding buffer. Fractions enriched in Ncd MC1 were identified by SDS/PAGE, pooled, and dialyzed in 20 mM Hepes, pH 7.2, with KOH, 0.1 mM EDTA, 0.1 mM EGTA, 5 mM magnesium acetate, 50 mM potassium acetate, 1 mM DTT, and 100 mM NaCl. The dialyzed protein was clarified and then concentrated by ultrafiltration, followed by loading onto an HPLC gel filtration column (Superose 10/300 GL; GE Healthcare) using a Beckman Coulter System Gold HPLC. The eluted homodimeric Ncd was collected and dialyzed against ATPase buffer: 20 mM Hepes, pH 7.2 with KOH, 0.1 mM EDTA, 0.1 mM EGTA, 5 mM magnesium acetate, 50 mM potassium acetate, 1 mM DTT, plus 5% sucrose. The dialyzed protein was clarified by ultracentrifugation, frozen as aliquots in liquid N_2, and stored at −80 °C. A single Ncd MC1 polypeptide contains the N-terminal 11 amino acid residues of bacteriophage T7 S10 protein (MASMTGGQQMG), two linker residues (RD), and the C-terminal 492 residues of Ncd, corresponding to amino acid sequence Leu^{209}–Lys^{700}. The predicted molecular weight based on amino acid sequence is 57,363 per polypeptide chain and 114,726 for the MC1 homodimer. Before each experiment, Ncd was clarified for 10 min at 4 °C (Beckman Coulter TLX ultracentrifuge, TLA-100 rotor, 313,000 × g), and the protein concentration was determined using the Bio-Rad protein assay with IgG as a protein standard. MT concentrations are reported as paclitaxel-stabilized tubulin polymer.

Pulse-Chase Kinetics of ATP Binding. To measure the kinetics of ATP binding (Fig. S2), the MT•Ncd complex (10 μM Ncd•ADP/30 μM MTs or 16 μM Ncd•ADP/30 μM MTs, syringe concentrations) was preformed and rapidly mixed in a chemical quench-flow instrument (RQF-3; KinTek Corp.) with MgATP plus trace [α-^{32}P]ATP and 200 mM KCl (syringe concentrations) from 5 to 400 ms (4–6). The reaction mixture was subsequently chased with 30 mM nonradiolabeled MgATP (syringe concentration) for 6 s (>10 ATP turnovers) and expelled from the instrument into a 1.5-mL tube containing 100 μL of 22 N formic acid. The acid terminated the reaction and released any nucleotide at the active site. The time of the chase allowed stably bound [α-^{32}P]ATP to be converted to [α-^{32}P]ADP•P_i, yet any [α-^{32}P]ATP unbound or bound loosely to the active site was diluted by the high concentration of nonradiolabeled ATP. One microliter of each reaction mixture was spotted onto a PEI-cellulose TLC plate (EMD Millipore) and developed with 0.6 M potassium phosphate buffer, pH 3.4, to separate [α-^{32}P]ATP from [α-^{32}P]ADP + P_i. The radiolabeled nucleotide was quantified using Image Gauge v4 software (FUJIFILM Science Laboratory). The concentration of [α-^{32}P]ADP product was plotted as a function of time, and the pre-steady-state burst equation (Eq. **S1**) was fit to each transient:

$$[\mathrm{ADP}] = A_0[1 - \exp(-k_b t)] + k_{slow} t, \qquad \textbf{[S1]}$$

where A_0 is the amplitude of the exponential burst phase, representing the stable formation of [α-^{32}P]ATP•motor complex that proceeded through ATP hydrolysis during the first ATP turnover, k_b is the observed rate of the exponential burst phase, and t is the time in seconds. The k_{slow} is the rate constant of the linear phase (μM·s^{-1}) and, when divided by the Ncd site concentration, corresponds to steady-state turnover. The observed exponential rates of each transient were plotted as a function of MgATP concentration, and Eq. **S2** was fit to the data:

$$k_{obs} = [K_1 k'_{+1}[\mathrm{ATP}]/(K_1[\mathrm{ATP}] + 1)], \qquad \textbf{[S2]}$$

where K_1 represents the equilibrium association constant for formation of the collision complex ($K_d = 1/K_1$), and k'_{+1} represents the first-order rate constant for the ATP-promoted isomerization to form the intermediate poised for ATP hydrolysis. The amplitude of each transient was plotted as a function of MgATP concentration, and the hyperbolic fit to the data provided the maximum amplitude, which can be related to the Ncd active sites in the experiment.

Acid-Quench Kinetics of ATP Hydrolysis. The pre-steady-state kinetic experiments to determine the time course of ATP hydrolysis were performed with a KinTek chemical quench-flow instrument. The MT•Ncd complex (10 μM Ncd•ADP/30 μM MTs, 16 μM Ncd•ADP/30 μM MTs, or 20 μM Ncd•ADP/30 μM MTs, syringe concentrations) was rapidly mixed with MgATP plus trace [α-^{32}P]ATP and 200 mM KCl (syringe concentrations) for times ranging from 5 to 400 ms. The reaction mixture was quenched with 22 N formic acid (syringe concentration), which terminated the reaction and released any nucleotide at the active site. The radiolabeled products [α-^{32}P]ADP and P_i were separated from [α-^{32}P]ATP by TLC and quantified using Image Gauge v4 software (FUJIFILM Science Laboratory). The concentration of product was plotted as a function of time, and Eq. **S1** was fit to the data, where A_0 is the amplitude of the exponential burst phase, representing the formation of [α-^{32}P]ADP•P_i at the active site during the first ATP turnover, k_b is the rate of the exponential burst phase, and t is the time in seconds. The constant

k_{slow} is the rate of the linear phase and, when divided by the Ncd site concentration, corresponds to steady-state turnover. The observed rate and amplitude of the exponential burst phase of each transient were plotted as a function of MgATP concentration, and a hyperbolic function was fit to each data set, providing the rate constant of ATP hydrolysis and the maximum amplitude of the exponential phase.

MT•Ncd Cosedimentation Assays. To determine the concentration of Ncd bound to the MTs in the preformed MT•Ncd complex for the pulse-chase (Fig. S2) and acid-quench (Fig. S3) experiments, equilibrium cosedimentation experiments were performed (3, 7). Reactions of 200 μL with MTs were formed at 8 μM Ncd•ADP/15 μM MTs or 16 μM Ncd•ADP/30 μM MTs in ATPase buffer plus 40 μM paclitaxel and incubated at room temperature for 30 min followed by centrifugation at 25 °C (Beckman Coulter TLX ultracentrifuge, TLA-100 rotor, 313,000 × g, 30 min). For each reaction, the supernatant was collected (top 100 μL of 200 μL with remaining 100 μL discarded). The MT pellet was resuspended in 100 μL of 5 mM $CaCl_2$ in buffer and incubated at 4 °C for 10 min. This step was repeated, and the two 100 μL $CaCl_2$ aliquots were combined. Laemmli 2× sample buffer was added to the supernatant (100 μL + 100 μL sample buffer) and resuspended pellet (200 μL + 200 μL sample buffer) for each reaction pair, followed by analysis by SDS/PAGE, in which the supernatant and pellet samples were loaded as equal volumes. The 8% acrylamide/2 M urea Coomassie Brilliant Blue R-250 stained gels were analyzed and quantified by Image Gauge v4 software.

MantATP Binding Following MT•Ncd Association. To mimic the reaction condition at the beginning of the cycle, 10 μM Ncd•ADP was rapidly mixed with 40 μM MTs plus varying concentrations of mantATP in the SF-2003 KinTek stopped-flow instrument (Fig. 2). Final concentrations: 5 μM Ncd•ADP sites, 20 μM MTs, and 0–15 μM mantATP (Invitrogen). The change in fluorescence of mantATP was monitored by excitation at 360 nm with detection at 450 nm using a 409-nm long-pass filter (Semrock, Inc.). The fluorescence of mantATP as well as mantADP is enhanced by the hydrophobic environment of the active site. A single exponential function was fit to each transient, and the observed rates obtained were plotted as a function of mantATP concentration. A hyperbolic function plus a *y*-intercept was fit to the data, providing the maximum rate constant of mantATP binding.

MantADP Release Kinetics from Head 1 and 2. The Ncd•mantADP complex (4 μM Ncd sites/8 μM mantADP) was rapidly mixed in the stopped-flow instrument with varying MT concentrations plus 1 mM MgATP. Final concentrations: 2 μM Ncd sites, 4 μM mantADP, 2–20 μM MTs, and 500 μM MgATP. The data were collected at a 2-s time domain to optimize capturing both the initial fast phase as well as the subsequent slow phase. Each transient (Fig. S4*A*) was fit to a double-exponential function. The observed rates for both the initial fast exponential phase and subsequent slow phase were each plotted as a function of ATP concentration (Fig. S4*B*). The hyperbolic fit to each provided the maximum rate constant of mantADP release from the first Ncd head to collide with the MT and the maximum rate constant associated with the second head's MT collision event and subsequent mantADP release.

Pre-Steady-State Kinetics of Phosphate Release. The kinetics of P_i release were determined using the *E. coli* phosphate-binding protein (PBP) that was developed as a P_i biosensor by introduction of a single cysteine into PBP at position 197 (A197C) and selectively labeled with the fluorophore MDCC (8, 9). The probe was excited at 436 nm with fluorescence emission at 474 nm detected via a 450-nm long-pass filter (Semrock, Inc.) in the stopped-flow instrument. MDCC-PBP binds phosphate rapidly (~136 $\mu M^{-1}\cdot s^{-1}$) and tightly (K_d ~0.1 μM), resulting in a fluorescence enhancement of approximately sevenfold that can be quantified (8–11). To remove free phosphate from the solutions and stopped-flow chamber, a "P_i mop" containing bacterial purine nucleoside phosphorylase (PNPase) and 7-methylguanosine (MEG) was used to sequester contaminating free phosphate as ribose-1-phosphate. The concentrations of MEG and PNPase were adjusted to 75 μM MEG and 0.025 U/mL PNPase in each syringe to achieve a rate of phosphate removal at 0.002 s^{-1} to prevent the Mop reaction from competing with MDCC-PBP.

To convert the MDCC-PBP fluorescence amplitude of each transient in volts into units of P_i concentration, a phosphate standard curve was used. MDCC-PBP in ATPase buffer with added 0.02 U/mL PNPase and 150 μM MEG (syringe concentrations) was rapidly mixed in the stopped-flow instrument with varying concentrations of KH_2PO_4. The initial exponential amplitude of each KH_2PO_4 transient in volts was plotted as a function of phosphate concentration to obtain a linear fit of the data. The phosphate-calibration curve was then used to convert the amplitude of each transient in Fig. 3 to units of concentration to relate to the total number of ATP hydrolysis and phosphate release events per Ncd site concentration in the experiment. The phosphate standard curve is performed with each experiment at the concentration of MDCC-PBP used to measure phosphate release from the MT•motor complex.

Parameter Estimation Method. The parameter estimation problem for the dynamic model of the Ncd powerstroke process (Fig. 4) can be mathematically formulated as follows:

$$\begin{aligned}
&\min_{\mathbf{P}} \sum_i \sum_k \left(\mathrm{F}_{ik} - \hat{\mathrm{F}}_{ik}\right)^2 \\
&\dot{\mathrm{X}}_1 = -k_1\mathrm{X}_1 + k_{-1}\mathrm{X}_2 \\
&\dot{\mathrm{X}}_2 = k_1\mathrm{X}_1 - k_{-1}\mathrm{X}_2 - k_2\mathrm{X}_2 M + k_{-2}\mathrm{X}_3 \\
&\dot{\mathrm{X}}_3 = k_2\mathrm{X}_2\mathrm{M} - k_{-2}\mathrm{X}_3 - k_3\mathrm{X}_3 \\
\text{s.t.}\quad &\dot{\mathrm{X}}_4 = k_3\mathrm{X}_3 - k_4\mathrm{X}_4\mathrm{M} \\
&\dot{\mathrm{X}}_5 = k_4\mathrm{X}_4\mathrm{M} \\
&\dot{\mathrm{M}} = -k_2\mathrm{X}_2 M + k_{-2}\mathrm{X}_3 - k_4\mathrm{X}_4\mathrm{M} \\
&\mathrm{F} = \lambda_1\mathrm{X}_3 + \lambda_2\mathrm{X}_4 + \lambda_3\mathrm{X}_5 \\
&\mathbf{P} = [k_1, k_{-1}, k_2, k_{-2}, k_3, k_4, \lambda_1, \lambda_2, \lambda_3]^{\mathrm{T}},\ p_j \geq 0\ \forall\, j = 1,2,\ \ldots, 9.
\end{aligned}$$

Here, F_{ik} and $\hat{F}_{ik}$ are the simulated and measured fluorescence at the *k*th sampling time under the *i*th experimental condition. Parameters *p* include k_1, k_{-1}, k_2, k_{-2}, k_3, k_4, λ_1, λ_2, and λ_3. The sampling times t_k are at 0.3, 0.5, 0.7, 0.9, 1.1, 1.3, 1.5, 1.6, 1.7, 1.8, 1.9, and 2.0 s. Data used for estimation were obtained from the mantATP binding experiments (Fig. 2), which were conducted at different initial concentrations of mantATP in the range of 0.5, 1.5, 2.5, 3.5, and 4.5 μM.

The parameter estimation problem is solved by applying an optimization algorithm that requires repeated evaluation of the objective function and its gradients by numerical integration of the ordinary differential equations (ODEs). In this work, *fmincon* (a MATLAB function) is used as the nonlinear programming (NLP) solver, and *ode45* (a MATLAB function) is used as the ODE solver.

1. Chandra R, Endow SA, Salmon ED (1993) An N-terminal truncation of the Ncd motor protein supports diffusional movement of microtubules in motility assays. *J Cell Sci* 104(Pt 3):899–906.
2. Chandra R, Salmon ED, Erickson HP, Lockhart A, Endow SA (1993) Structural and functional domains of the *Drosophila* Ncd microtubule motor protein. *J Biol Chem* 268(12):9005–9013.
3. Foster KA, Correia JJ, Gilbert SP (1998) Equilibrium binding studies of non-claret disjunctional protein (Ncd) reveal cooperative interactions between the motor domains. *J Biol Chem* 273(52):35307–35318.
4. Foster KA, Gilbert SP (2000) Kinetic studies of dimeric Ncd: Evidence that Ncd is not processive. *Biochemistry* 39(7):1784–1791.
5. Foster KA, Mackey AT, Gilbert SP (2001) A mechanistic model for Ncd directionality. *J Biol Chem* 276(22):19259–19266.
6. Gilbert SP, Mackey AT (2000) Kinetics: A tool to study molecular motors. *Methods* 22(4):337–354.
7. Chen CJ, Rayment I, Gilbert SP (2011) Kinesin Kar3Cik1 ATPase pathway for microtubule cross-linking. *J Biol Chem* 286(33):29261–29272.
8. Brune M, Hunter JL, Corrie JE, Webb MR (1994) Direct, real-time measurement of rapid inorganic phosphate release using a novel fluorescent probe and its application to actomyosin subfragment 1 ATPase. *Biochemistry* 33(27):8262–8271.
9. Brune M, et al. (1998) Mechanism of inorganic phosphate interaction with phosphate binding protein from *Escherichia coli*. *Biochemistry* 37(29):10370–10380.
10. Gilbert SP, Webb MR, Brune M, Johnson KA (1995) Pathway of processive ATP hydrolysis by kinesin. *Nature* 373(6516):671–676.
11. Klumpp LM, Hoenger A, Gilbert SP (2004) Kinesin's second step. *Proc Natl Acad Sci USA* 101(10):3444–3449.

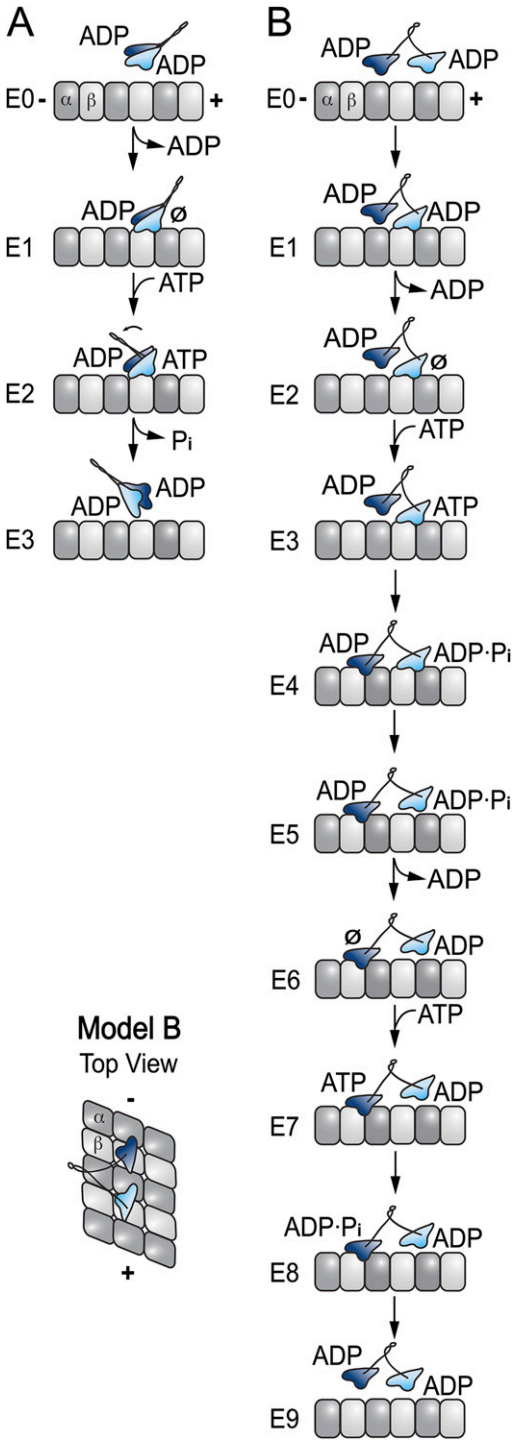

Fig. S1. Alternative Ncd ATPase schemes. (*A*) The Wendt et al. (1) and Endres et al. (2) model proposes that only one Ncd head interacts with a microtubule with one ATP turnover event per powerstroke. The cycle is initiated when one head of dimeric Ncd collides with the MT, followed by ADP release (E0–E1). ATP binding to the nucleotide-free head triggers the ~70° rotation of the coiled-coil stalk toward the MT minus end (E1–E2). ATP hydrolysis occurs followed by phosphate release and Ncd dissociation from MT (E2–E3). (*B*) The scheme proposed by Foster et al. (3) was based on the assumption that both Ncd heads interact with the MT and both bind and hydrolyze ATP. The cycle begins with MT collision followed by ADP release (E0–E2). ATP binding followed by ATP hydrolysis triggers the second head to bind to the MT (E3–E4). This model predicts that rearward head detachment occurs as the ADP•P_i state, triggering tight MT binding of the leading head followed by ADP release (E5–E6). Another ATP turnover is required for detachment of Ncd from the MT (E7–E9). This model differs from the Wendt et al. (1) and Endres et al. (2) model in that both heads of the Ncd dimer interact with the MT with two ATP turnover events per powerstroke.

1. Wendt TG, et al. (2002) Microscopic evidence for a minus-end-directed power stroke in the kinesin motor Ncd. *EMBO J* 21(22):5969–5978.
2. Endres NF, Yoshioka C, Milligan RA, Vale RD (2006) A lever-arm rotation drives motility of the minus-end-directed kinesin Ncd. *Nature* 439(7078):875–878.
3. Foster KA, Mackey AT, Gilbert SP (2001) A mechanistic model for Ncd directionality. *J Biol Chem* 276(22):19259–19266.

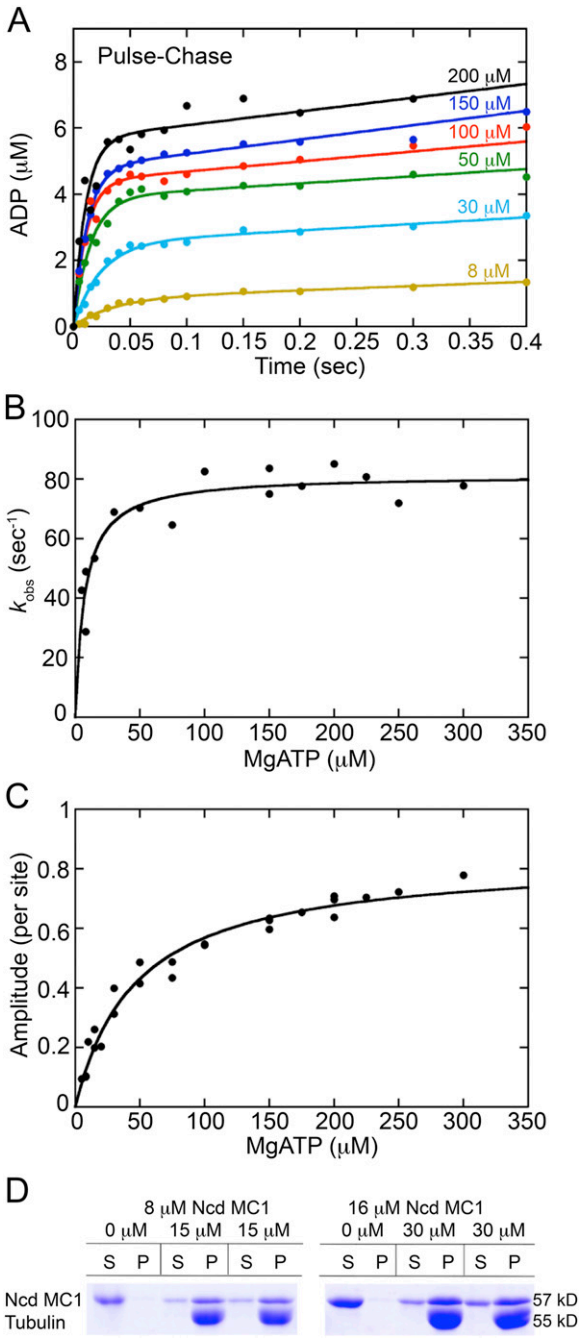

Fig. S2. Pulse-chase kinetics of ATP binding. The MT•Ncd complex was rapidly mixed in the chemical quench-flow instrument with increasing concentrations of MgATP + trace [α-^{32}P]ATP and 200 mM KCl, followed by a chase with 30 mM unlabeled MgATP (syringe concentrations). Final concentrations: 5 μM Ncd•ADP/15 μM MTs or 8 μM Ncd•ADP/15 μM MTs, 0–300 μM [α-^{32}P]ATP, and 100 mM KCl. (*A*) Representative transients for ATP binding show an initial exponential formation of [α-^{32}P]ADP•P_i during the first ATP turnover followed by a linear phase of product formation representing subsequent ATP turnovers. Final MT•Ncd complex concentrations: 8 μM Ncd•ADP/15 μM MTs. (*B*) The observed rates of the pre-steady-state exponential phase determined for individual transients were plotted as a function of MgATP concentration, and the Eq. **S2** fit provided the maximum $k_b = 81.3 \pm 2.6$ s^{-1} and $K_{d,ATP} = 7.1 \pm 0.03$ μM. (*C*) The amplitude of each exponential phase was normalized to the concentration of Ncd sites and plotted as a function of MgATP concentration. A hyperbolic fit to the data provided the maximum burst amplitude of 0.84 ± 0.03 μM ADP•P_i per site and $K_{d,ATP} = 47 \pm 5.2$ μM. The data in *B* and *C* represent multiple experiments. (*D*) The MT•Ncd complex used in the pulse-chase experiments was evaluated by cosedimentation assays. The supernatant (S) and pellet (P) for each reaction are shown with the concentration of MTs indicated above each pair. Approximately 80% of the total Ncd pelleted with MTs at the conditions of the pulse-chase experiments, indicating that all MT-associated Ncd motor heads did bind and hydrolyze ATP during the first ATP turnover.

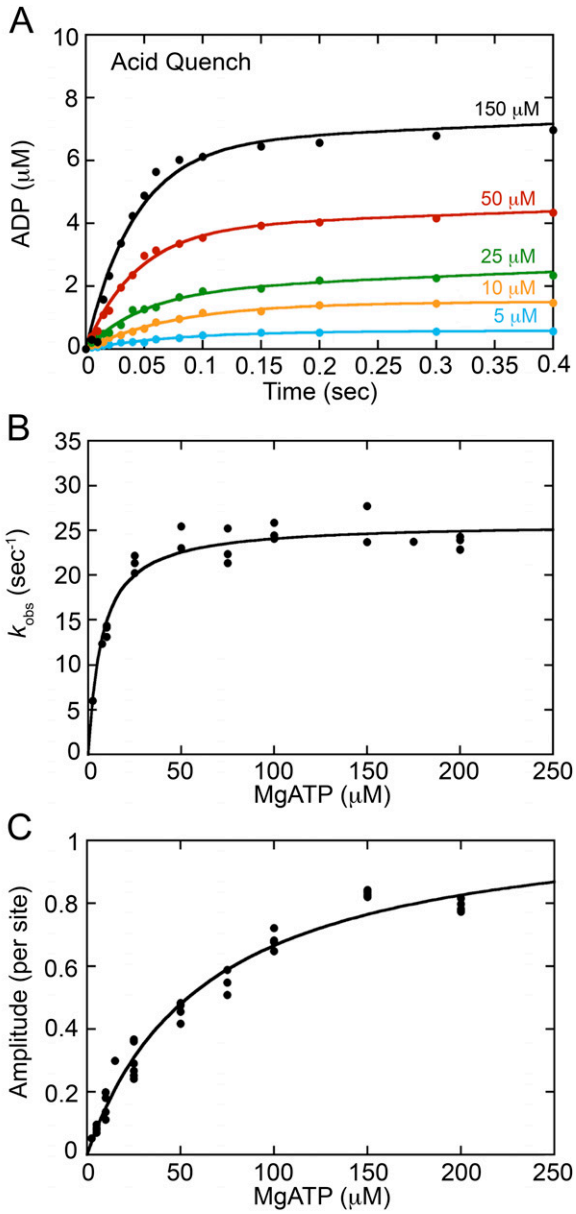

Fig. S3. Acid-quench kinetics of ATP hydrolysis. The preformed MT•Ncd complex was rapidly mixed in the chemical quench-flow instrument with increasing concentrations of MgATP + trace [α-^{32}P]ATP and 200 mM KCl (syringe concentrations). Final concentrations: 5 μM Ncd•ADP/15 μM MTs, 8 μM Ncd•ADP/15 μM MTs, or 10 μM Ncd•ADP/15 μM MTs, 0–300 μM [α-^{32}P]ATP, and 100 mM KCl. (*A*) Representative transients show an initial exponential phase of [α-^{32}P]ADP•P_i during the first ATP turnover followed by a linear phase of product formation representing subsequent ATP turnovers. Final MT•Ncd complex concentrations: 8 μM Ncd•ADP/15 μM MTs. (*B*) The observed rates of the presteady-state exponential phase determined for individual transients were plotted as a function of MgATP concentration, and the hyperbolic fit to the data provided the maximum $k_b = 26 \pm 0.6$ s^{-1} and $K_{d,ATP} = 7.2 \pm 0.9$ μM. At high ATP concentrations, ATP hydrolysis becomes rate-limiting; therefore, the maximum k_b represents the rate constant for ATP hydrolysis. (*C*) The amplitude of the exponential phase for each transient was normalized to the concentration of Ncd sites and plotted as a function of MgATP concentration. The hyperbolic fit to the data provided $A_{max} = 1.09 \pm 0.04$ μM ADP•P_i per site and $K_{d,ATP} = 63.7 \pm 6$ μM. The acid-quench amplitude data also support the argument that all MT-associated Ncd motor heads did bind and hydrolyze ATP during the first ATP turnover.

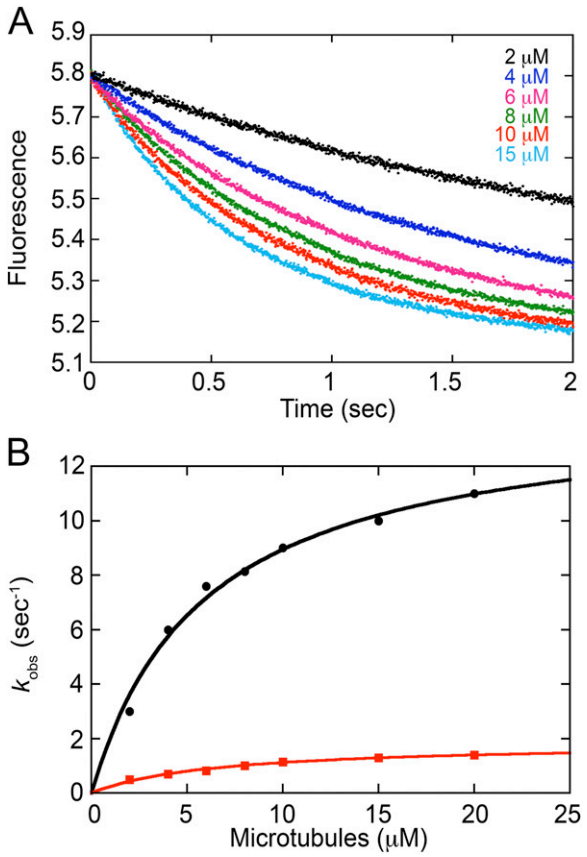

Fig. S4. MantADP release kinetics from Ncd heads 1 and 2. The Ncd•mantADP complex (4 μM Ncd sites/8 μM mantADP) was rapidly mixed in the stopped-flow instrument with increasing concentrations of MTs plus 1 mM MgATP. Final concentrations: 2 μM Ncd sites/4 μM mantADP, 2–20 μM MTs, and 500 μM MgATP. (*A*) Representative transients are biphasic with an initial rapid phase of fluorescence quenching followed by a slow phase. Each transient was fit to a double-exponential function, which provided the observed rates of mantADP release from each exponential phase. (*B*) The observed rates for the initial fast phase of mantADP release associated with the first head that collides with the MT and the subsequent slow phase of mantADP release associated with the second head that collides with the MT were plotted as a function of MT concentration. The hyperbolic fit of each data set provided a maximum rate constant for the fast phase at 14.2 ± 0.7 s^{-1} and the slow phase at 1.85 ± 0.1 s^{-1}. The amplitudes associated with each phase were not equivalent with only ~25% of the total amplitude associated with the fast phase. The decrease in the amplitude associated with the initial fast phase results because of the relatively weak ADP affinity for one of the Ncd heads in solution and previously proposed to be the head that initially collides with the MT (1) as well as the time domain used to capture both the fast and slow exponential phases. These results are consistent with rates reported previously for mantADP release upon MT collision and ATP-promoted head 2 mantADP release (Table S1) (1).

1. Foster KA, Mackey AT, Gilbert SP (2001) A mechanistic model for Ncd directionality. *J Biol Chem* 276(22):19259–19266.

Table S1. Experimentally determined constants for the MT•Ncd ATPase

Reaction step	Constants
mantATP binding following MT•Ncd association	$k_{max} = 4.4 \pm 0.2\ s^{-1}$
	$k_{off} = 1.8 \pm 0.1\ s^{-1}$
	$K_{1/2,mantATP} = 9.4 \pm 1.4\ \mu M$
mantATP binding to the MT•Ncd complex (from ref. 1)	$k_{max} = 2.3 \pm 0.1\ \mu M^{-1} \cdot s^{-1}$
	k_{-1} not observed
ATP binding (pulse-chase)	$K_1 = 0.14 \pm 0.03\ \mu M^{-1}$
	$k_{+1}' = 81.3 \pm 2.6\ s^{-1}$
	$K_1 k_{+1}' = 11.4 \pm 0.08\ \mu M^{-1} \cdot s^{-1}$
	$K_{d,ATP} = 7.1\ \mu M$
	$A_0 = 0.84 \pm 0.03\ \mu M$ ADP•P_i per Ncd site
	$K_{d,ATP} = 47 \pm 5.2\ \mu M$
ATP hydrolysis (acid quench)	$k_{max} = 26 \pm 0.6\ s^{-1}$
	$K_{d,ATP} = 7.2 \pm 0.9\ \mu M$
	$A_0 = 1.09 \pm 0.04\ \mu M$ ADP•P_i per Ncd site
	$K_{d,ATP} = 63.7 \pm 6\ \mu M$
MT•Ncd association (from ref. 1)	$k_{max} = 0.7 \pm 0.1\ \mu M^{-1} \cdot s^{-1}$
	$k_{-1} = 2.7 \pm 0.6\ s^{-1}$
mantADP release from head 1 (from ref. 2)	$k_{max} = 17.8 \pm 1.6\ s^{-1}$
	$K_{1/2,MT} = 2.2 \pm 2.0\ \mu M$
mantADP release from head 2 (from ref. 2)	$k_{max} = 1.4 \pm 0.02\ s^{-1}$
	$K_{1/2,ATP} = 0.64 \pm 0.06\ \mu M$
Phosphate release following MT•Ncd association	$k_{max} = 2.9 \pm 0.1\ s^{-1}$
	$K_{1/2,ATP} = 16 \pm 1\ \mu M$
	$A_{0,max} = 5.7 \pm 0.25\ \mu M\ P_i$ (~1.1 P_i/Ncd site)
Phosphate release from the MT•Ncd complex	$k_{max} = 14.3 \pm 0.3\ s^{-1}$
	$K_{1/2,ATP} = 23.3 \pm 2.3\ \mu M$
	$A_{0,max} = 1.1 \pm 0.01\ \mu M\ P_i$ (~0.44 P_i/Ncd site)
ATP-promoted MT•Ncd dissociation (from ref. 1)	$k_{max} = 13.1 \pm 0.6\ s^{-1}$
	$K_{1/2,ATP} = 18.7 \pm 4.1\ \mu M$
Steady-state parameters (from ref. 3)	$k_{cat} = 2.1 \pm 0.2\ s^{-1}$
	$K_{m,ATP} = 23.1 \pm 1.5\ \mu M$
	$K_{1/2,MT} = 18.3 \pm 5.1\ \mu M$

Errors are ±SEM.

1. Foster KA, Gilbert SP (2000) Kinetic studies of dimeric Ncd: Evidence that Ncd is not processive. *Biochemistry* 39(7):1784–1791.
2. Foster KA, Mackey AT, Gilbert SP (2001) A mechanistic model for Ncd directionality. *J Biol Chem* 276(22):19259–19266.
3. Foster KA, Correia JJ, Gilbert SP (1998) Equilibrium binding studies of non-claret disjunctional protein (Ncd) reveal cooperative interactions between the motor domains. *J Biol Chem* 273(52):35307–35318.